*Research Article*

MOLECULAR PAIN

Molecular Pain
Volume 15: 1–16

DOI: 10.1177/1744806918823477
journals.sagepub.com/home/mpx
SAGE

# Inhibiting STAT3 in a murine model of human breast cancer-induced bone pain delays the onset of nociception

**Katja Linher-Melville[1], Manu Sharma[1], Peter Nakhla[1], Elena Kum[1], Robert Ungard[1], Ji Park[2], David Rosa[2], Patrick Gunning[2], and Gurmit Singh[1]**

## Abstract

Aggressive breast cancer subtypes utilize system $x_c^-$, a membrane antiporter, to import cystine for glutathione synthesis and maintenance of redox homeostasis, in turn releasing glutamate as a metabolic pro-nociceptive by-product. Metastatic breast cancers establish themselves at distal sites including bone, where changes in extracellular glutamate levels contribute to cancer-induced bone pain. We previously established that stearically blocking system $x_c^-$ activity with sulfasalazine delays the onset of nociceptive behaviours and that xCT, the functional antiporter subunit, is positively regulated by signal transducer and activator of transcription 3 (STAT3). In the current investigation, a murine xenograft cancer-induced bone pain model was applied to examine whether pharmacological inhibition of phosphorylated STAT3 (pSTAT3) induces changes in nociception. A high glutamate-releasing, xCT/pSTAT3 over-expressing human breast cancer cell line was selected for injection into the distal epiphysis of the right femur of female nude mice. A 14-day regimen of intraperitoneal injections with either vehicle or the novel STAT3 inhibitor DR-1–55 commenced three weeks after initial intrafemoral bone injection. Nociceptive behaviours were temporally monitored by automated von Frey, dynamic weight bearing and open-field testing for the duration of the study, beginning at the baseline. Prior to sacrifice and at ethical end point, tumour-induced osteolytic lesions were radiographically assessed. Treatment with DR-1–55 significantly delayed the onset and severity of spontaneous and induced nociceptive behaviours, also decreasing human *SLC7A11* (*xCT*) mRNA levels in tumour-bearing limbs without altering osteolysis. In addition, two pro-inflammatory cytokines released by this cell line, interleukin 6 and interleukin 1β, were also down-regulated at the mRNA level in response to DR-1–55 treatment in vivo, with lower human interleukin 6 levels detected in the host circulation. This study demonstrates that targeting pSTAT3 may be a viable therapeutic means to manage cancer-induced bone pain, alone or in combination with stearic system $x_c^-$ blockers.

**Keywords**

cancer pain, glutamate, STAT3, system $x_c^-$, cytokines

Date Received: 14 September 2018; revised: 14 November 2018; accepted: 27 November 2018

## Introduction

Cancer is the leading world-wide cause of morbidity and mortality, with 14 million new cases and 8 million cancer-related deaths reported in 2012.[1] Up to 70% of cancer patients experience pain,[2] with greater than 33% describing pain as a distressing and intolerable aspect of the disease.[3] Adequate pain management has been associated with clinically relevant improvements in patient quality of life.[4] In an effort to intensify research into its underlying mechanisms, including pain due to bone metastases,[5] the International Association for the Study of Pain launched 2008 as the Global Year Against Cancer Pain. Increased opioid prescriptions and intensified research into developing new therapeutic analgesic agents raised expectations that the prevalence of cancer

[1]Department of Pathology and Molecular Medicine, McMaster University, Hamilton, Ontario, Canada
[2]Department of Chemical and Physical Sciences, University of Toronto Mississauga, Mississauga, Ontario, Canada

**Corresponding Author:**
Gurmit Singh, Department of Pathology and Molecular Medicine, McMaster University, Hamilton, Ontario L8S 4L8, Canada.
Email: singhg@mcmaster.ca

pain would decline. Analysis of data from 1966–2005 revealed the prevalence of pain in cancer patients after curative therapy to be 33%, 59% in those undergoing anti-cancer treatment, 64% in those with advanced, metastatic or terminal disease and 53% at all stages of cancer.[2] However, a systematic review and meta-analysis of data collected during the period from 2005–2014 revealed no improvements, with a 39.3% prevalence of pain in cancer patients after curative therapy, 55.0% in those undergoing anti-cancer treatment, 66.4% in those with advanced disease and 50.7% at all stages of cancer,[6] indicating that pain continues to be a prevalent co-morbidity. Given that opioids are not a sustainable solution to increase patient quality of life in terms of daily functionality, there remains a clinical need to adopt new pharmacological agents that produce tolerable side effects.[7]

In terms of breast cancer, an estimated 1.4 million women and men are diagnosed each year, with skeletal metastases that occur in 65% to 75% of breast cancer patients[8] representing a source of significant pain.[9] The severity of cancer-induced bone pain (CIBP) varies considerably, with some patients experiencing minimal symptoms while others describe deep and penetrating pain, which may be accompanied by sporadic episodes of intractable discomfort.[8] The variable nature of CIBP may be cancer subtype-dependent, and influenced, at least in part, by the specific metabolic profile of metastatic cells, which may also be linked with their tumour growth potential within the bone microenvironment. Currently, analgesic options for treating CIBP are limited primarily to non-steroidal anti-inflammatories and opioids, with the latter further impacting patient quality of life.[9]

Our group has been actively exploring the contribution of glutamate derived from peripherally induced skeletal tumours to CIBP in relevant animal models. In the bone, changes in extracellular glutamate levels affect osteoclasts, osteocytes and osteoblasts.[10] Exogenous glutamate also acts as an excitatory neurotransmitter, stimulating peripheral afferents to evoke nociceptive responses.[11,12] We and others have shown that stearic blockers (sulfasalazine, capsazepine) of system $x_c^-$, a membrane antiporter present on particularly aggressive cancer cells that specifically mediates the release of excess intracellularly produced glutamate in exchange for cystine uptake, delay the onset or ameliorate the severity of nociceptive behaviours in preclinical CIBP models.[13–15] Of additional relevance, it has been shown that inhibiting system $x_c^-$ activity with sulfasalazine decreases tumour growth, which is of interest in targeting cancer subtypes associated with a particularly poor prognosis.[16] For example, sulfazalazine markedly reduced the growth and viability of human pancreatic cancer cells in vitro as well as xenograft growth in immunodeficient mice.[17] In human non-Hodgkin's lymphoma and rat Nb2 lymphoma cultures, this agent potently blocked system $x_c^-$ and induced high growth-inhibitory activity in vitro, and its intraperitoneal (IP) administration to rats inhibited continued growth of Nb2 lymphoma transplants.[18] However, the clinical application of sulfasalazine to treat CIBP is not being actively pursued, given its rapid metabolism into two bioactive constituents in vivo, reducing its potency in blocking system $x_c^-$ activity.

Up-regulated functional antiporter activity may be indicative of a shift in cancer cell metabolism towards glutaminolysis to support the production of intracellular glutamate. Glutamine dependency indirectly supports cystine acquisition through system $x_c^-$, which is present on a third of triple-negative human breast carcinomas.[16] The ability to take up cystine presents an additional growth advantage in the form of increased reactive oxygen species (ROS) neutralization, which is important, given that, as by-products of dysregulated metabolism, these molecules disrupt intracellular redox balance.[19] This is countered in part by the antioxidant glutathione, with its synthesis dependent on an adequate intracellular pool of cysteine, which is refreshed through continuous system $x_c^-$-mediated cystine uptake.[20] Taken together, targeting system $x_c^-$ to ameliorate CIBP provides several advantages, both as an anti-nociceptive strategy by limiting glutamate release and as a means of controlling tumour growth, which itself may be associated with bone pain by inducing mechanical pressure as well as fractures.

Interestingly, CIBP includes inflammatory components, and pro-inflammatory cytokines such as IL-1β have been linked with the expression of xCT, the functional component of system $x_c^-$, at the protein level.[21] Down-regulating *xCT* at the mRNA level may therefore provide another means of therapeutically targeting cancer cell-mediated glutamate release. Signal transducer and activator of transcription (STAT) proteins are constitutively active in many human cancers, including lymphomas, pancreatic cancers and aggressive breast cancers, play a role in cancer inflammation,[22] affect redox homeostasis[23] and regulate xCT.[24,25] Phospho-STAT3 (pSTAT3) is constitutively active in triple-negative human MDA-MB-231 breast cancer cells, which release significant levels of glutamate and have been used by our group to induce CIBP xenograft models.[13,14] We have shown that after 24 h in the presence of the STAT3/STAT5 pathway inhibitor SH-4–54,[26] *xCT* mRNA levels were up-regulated in MDA-MB-231 cells through a ROS-mediated stress response.[24] After the initial spike in ROS levels, a sustained block of pSTAT3, achieved through continued culture in the presence of SH-4–54, induced significant down-regulation of *xCT* mRNA in clonally selected MDA-MB-231 cell lines.[25] In contrast, human SH-4–54-selected T47D breast

cancer clones exhibited significant increases in *xCT* mRNA levels relative to parental cells,[25] which do not normally express pSTAT3 in the absence of relevant growth factor stimulation. This suggested that *xCT* and STAT3 are positively correlated, and that targeting STAT3 in aggressive breast cancer cells could be another means of down-regulating system $x_c^-$.

In the present investigation, (1) the pSTAT3/xCT over-expressing T47D cell line described above was applied as a tool to examine the contribution of this aggressive cellular signature to nociceptive responses in a CIBP xenograft model and (2) the putative anti-nociceptive effects of DR-1–55, a small-molecule inhibitor of STAT3 with enhanced in vivo stability and bioavailability compared to SH-4–54,[27] were examined. We hypothesized that two weeks of daily DR-1–55 administration would significantly down-regulate *xCT* mRNA levels in bone tumours to ameliorate nociceptive behaviours.

## Methods

### Cell culture

Mycoplasma-free MDA-MB-231 and T47D cell lines clonally derived through chronic treatment of wild-type human MDA-MB-231 and T47D breast carcinoma cells with SH-4–54 (referred to as clones; described in detail in Linher-Melville et al.[25]), respectively (parental cells originally purchased from the American Type Culture Collection, Manassas, VA, USA and cultured to passage-match clones) were maintained at sub-confluence (approximately 80%–90%) in a humidified incubator with 5% $CO_2$ at 37°C using Dulbecco's Modified Eagle Medium (DMEM; MDA-MB-231s) or Roswell Park Memorial Institute medium (RPMI; T47Ds) supplemented with 10% fetal bovine serum and 1% antibiotics/antimycotics. SH-4–54 was not supplemented to clones for any of the experiments conducted in this study.

### Secretome analysis

MDA-MB-231 and T47D clones, along with respective wild-type counterparts, were plated at optimal densities and cultured in 10-cm dishes. After 48 h, all cells were approximately 90% confluent. Conditioned media was collected and centrifuged at 500*g* for 5 min at 4°C, and cell-free supernatants were stored at −80°C. Corresponding trypsinized cell counts were determined manually by haemocytometer. For each cell type, three (n = 3) separate culture media samples were collected for analysis. The concentration of 54 cytokines, chemokines, neurotrophins and growth factors (EGF, Eotaxin-1, FGF-2, Flt-3L, Fractalkine, G-CSF, GM-CSF, GRO (alpha), IFNalpha2, IFNgamma, IL-1alpha, IL-1beta, IL-1ra, IL-2, IL-3, IL-4, IL-5, IL-6, IL-7, IL-8, IL-9, IL-10, IL-12 (p40), IL-12 (p70), IL-13, IL-15, IL-17A, IL-18, IP-10, MCP-1, MCP-3, MDC, MIP-1alpha, MIP-1beta, PDGF-AA, PDGF-AB/BB, RANTES, sCD40L, TGFalpha, TNFalpha, TNFbeta, VEGF-A, AGRP, CNTF, ACTH, FSH, LH, GH, Prolactin, TSH, BDNF, TGF-beta1, TGF-beta2, TGF-beta3), several of which have been implicated in neuropathic or inflammatory pain conditions, were assessed in the human breast cancer cell supernatants sourced to Eve Technologies (Calgary, Alberta) via same-day shipment on dry ice. Quantitative assays were based on xMAP technology, allowing for simultaneous detection of multiple analytes within a single sample. Results were normalized to total cell counts. Aliquots of DMEM and RMPI supplemented with 10% fetal bovine serum and 1% antibiotics/antimycotics served as assay blanks.

### Glutamate assay

Using the same 48 h cell culture supernatant samples subjected to secretome analysis (n = 3), glutamate released from each cell line was quantified using the Amplex Red L-glutamic acid assay kit (Invitrogen/Molecular Probes, Eugene, OR) following a 1:10 dilution with 1× assay reaction buffer. Readings obtained using a CytoFluor Series 4000 Fluorescence Multi-Well Plate Reader (PerSeptive Biosystems, Framingham, MA) validated previous findings in which the cell lines were still undergoing culture in SH-4–54.[25] The Amplex Red assay quantifies glutamate levels by measuring the fluorescent reaction product, resorufin, which is produced proportionately to the amount of glutamate in each test sample. Results were normalized to total cell counts. DMEM and RMPI supplemented with 10% fetal bovine serum and 1% antibiotics/antimycotics served as assay blanks.

### Drug reconstitution

DR-1–55 was reconstituted by dissolving the lyophilate (806.68 g/mol) in sterile 1% v/v dimethyl sulfoxide, 5% v/v Tween 80 and 50% v/v polyethylene glycol 400 (PEG-400), with the remaining volume adjusted with cell culture grade sterile $H_2O$ to a final concentration of 5 mg/mL (6.2 mM). The solution was heated to 50°C for 10 min, ensuring complete resuspension, and stored at 4°C. Vehicle corresponded to diluent only.

### In vivo experiments

All protocols developed for animal studies reported in the current investigation were approved by the Animal Research Ethics Board of McMaster University and adhered to Canadian Council on Animal Care

guidelines. Upon arrival at the Central Animal Facility (CAF), four- to six-week-old female athymic NU/J mice (Jackson Laboratories) were acclimatized to their environment prior to handling by the experimental tester. To ensure lack of bias, animals were randomized into groups with the tester blinded with regard to treatment (type of cancer cell injected, administration of vehicle or drug). For consistency, measurements and behavioural tests were performed by the same tester throughout a study.

### Subcutaneous model

In vivo growth potential was assessed as described for MDA-MB-231 cells and their corresponding clones.[25] The subcutaneous xenograft model was induced by injecting $4 \times 10^6$ T47D wild-type cells or T47D clones along the right flank of each mouse ($n = 4$ per group). Tumour volume (length $\times$ width $\times$ height $\times$ 0.5236) was measured using a caliper two to three times per week beginning on day 10 post-injection (when tumours first became apparent) until day 31 (end point).

### CIBP model

Three days before human breast cancer cell bone injections, mice were anaesthetized by gaseous isoflurane inhalation to facilitate subcutaneous implantation of 21 day-release estrogen pellets containing 0.25 mg of 17β-estradiol in the cervical region. On the day of bone injections, animals were anaesthetized, injected subcutaneously with 50 µL of a 1:10 solution of buprenorphine and laid supine while the right rear knee was bent at 90° to facilitate patellar clearance. A 1 mL insulin syringe was filled with 50 µL of a $1 \times 10^6$ cancer cell suspension in sterile PBS and fitted to a 26-gauge needle, which was placed between the medial and lateral condyles of the distal epiphysis of the right femur and gently rotated to penetrate the bone. The cell suspension was injected at a steady rate to minimize marrow displacement. At the time of intrafemoral injections, T47D clones were at passage 21, having been thawed from a passage 18 cell stock maintained in liquid nitrogen. Wild-type T47D cells, where appropriate, were passage-matched. Each cancer cell group corresponds to $n = 8$ mice, while three additional animals were injected with $1 \times 10^6$ heat-freeze/thaw-inactivated T47D clones (sham) suspended in 50 µL of sterile PBS to mimic disturbances to the bone microenvironment associated with surgical manipulation or the presence of foreign cellular material. Animals were group-housed, five per cage. All cells were tested for post-surgical viability via trypan blue staining and microscopy.

### DR-1–55 pharmacokinetics

A pharmacokinetic study was carried out in 3 six- to eight-week-old male CD-1 mice with IP administration of 25 mg/kg of DR-1–55, with approximately 0.02 mL of blood being collected at 5-min, 15-min, 30-min, 1-h, 2-h, 4-h, 8-h and 24-h intervals post-dosing. Each blood sample was transferred into plastic microcentrifuge tubes containing heparin-Na and centrifuged at 4000*g* for 5 min at 4°C. Plasma samples were stored at −75°C prior to analysis of DR-1–55 concentrations using a LC-MS/MS method. WinNonlin (PhoenixTM, version 6.1) software was used for pharmacokinetic calculations. The following parameters were calculated from the plasma concentration versus time data: $T_{1/2}$ (h), $T_{max}$ (h), $C_{max}$ (ng/mL), $AUC_{last}$ (h · ng/mL), $AUC_{inf}$ (h · ng/mL), AUC Extr (%), MRT (h) and AUC/D (h · mg/mL).

### Drug administration for the CIBP study

Beginning on day 21 post-cancer cell injection into the bone, $n = 10$ mice (one sham and nine cancer cell-injected per treatment group) were subjected to 14 consecutive days of IP injection with either vehicle or 25 mg/kg per day of DR-1–55. One additional sham was left untreated (no IP injections), for a total of three animals without a bone tumour. The site of daily IP injection was altered from left to the right to avoid excessive stimulation of a single locus.

### Behavioural tests

Baseline behavioural measurements were obtained after acclimatization to the CAF, one week prior any surgical procedures. After bone injections, behavioural data were collected twice a week at consistent times on predefined days. Spontaneous nociceptive behaviours were scored using the Dynamic Plantar Aesthesiometer (DPA; Ugo Basile, Comerio, Italy), Dynamic Weight Bearing (DWB) apparatus (Bioseb, France) and Open-field testing. For all tests, data derived from animals that failed to develop a tumour, as assessed by radiographic imaging, was excluded from final analyses.

### DPA test

The DPA test measures the force, in grams, of paw withdrawal caused by a mechanical stimulus to the plantar surface of the paw. It employs an electronic actuator that vertically displaces a Von Frey filament, prompting an electronic assessment of induced hyperalgesia and mechanical allodynia. Subjectivity of the operator is reduced by allowing for a constant rate of change in the force applied by the filament. The maximum force was set to reach 15 g over a maximum time of 5 s.

Animals were allowed an approximate 5-min interval to acclimate to the DPA chamber, and testing was performed four times on the tumour-bearing hind paw. The threshold force at paw withdrawal was expressed as a mean of the four values, with a reduction in force indicating increased hyperalgesia/allodynia. This was characteristic of a reflexive, voluntary withdrawal in response to the stimulus and was therefore used as an indirect measurement of nociception.

### DWB test

The DWB test includes a video component (Grandtech webcam) attached by a fixed rod above a Plexiglas-enclosed sensor pad used to track differential paw distribution by filming an animal's movement over time. This system represents evoked nociception without restraint-associated stress, allowing an evaluation of spontaneous nociceptive behaviour by measuring changes in an animal's postural equilibrium (weight distribution) based on the average pressure placed on each paw. Mice were allowed 1 min to acclimate to the pre-calibrated DWB apparatus, with 5 min of total video footage captured per animal. The analysis software recognizes each paw on the sensor pad, accounting for the weight of each animal to generate a normalized % weight (in grams) of rear right paw usage. Manual validation by a blinded assessor was required to ensure a match in spatial orientation under the following parameters: low weight threshold of 0.75 g; weight threshold of 1 g; surface threshold of two units and minimum nb image of 3.

### Open-field test

Open-field observational testing was conducted immediately after the DWB test, with each animal remaining in the enclosed Plexiglas chamber. Visual pain scoring followed a predefined criterion based on favouring of the tumour-bearing limb, with scores from 4 to 0: (4) normal limb use, (3) a pronounced limp during locomotive activity, (2) a pronounced limp and notable guarding behaviour when stationary, (1) partial non-use of the limb in locomotive activity and evident pivotal favouring and (0) complete lack of limb use. A score of (0) is an automatic criterion for sacrifice as outlined in our animal utilization protocol (AUP) ethical clause. Animals were observed for a total of 1.5 min.

### Radiographic imaging and lesion scoring

High-resolution X-ray images at 3× magnification were taken of each tumour-bearing limb on two experimental days (Faxitron X-ray System MX-20, Wheeling, IL). One set was obtained on day 29 via interim gaseous anesthetization, with mice imaged sequentially by cage grouping, and the other of flash-frozen limbs post-sacrifice (day 34). To compare the extent of osteolytic lesions, a radiographic scoring system was employed to evaluate bone density loss within the distal epiphysis of each tumour-bearing femur. Using a 0 to 3 scale, each femur was rated by a blinded assessor according to specific designations: (0) normal bone, with no visible lesion, (1) minor loss of bone density with a minimal lesion, (2) moderate to substantial loss of bone density with the lesion limited to the trabeculae and cortex and (3) substantial loss of bone density with the lesion including periosteal involvement or fracture.[14]

### Crystal violet assay

Changes in cell number in response to DR-1–55 treatment were quantified by crystal violet staining. Approximately 10,000 cells were plated into each well of a 96-well plate. After a 24-h adherence period, cells were treated with vehicle or DR-1–55, ranging from 0.24–3.87 μM, for 72 h. Media was aspirated from each well and cells were fixed in formalin for 30 min, followed by a 10-min incubation in 0.25% crystal violet in 25% methanol. After rinsing excess stain from the wells with deionized water and air-drying, the content of each well was solubilized in a solution of 0.05 M $NaH_2PO_4$ in 50% ethanol. Plates were read on a Biotek spectrophotometer at 570 nm. Cell numbers were extrapolated based on standard growth curves prepared for each cell line.

### Western blotting

Western blotting and densitometry were carried out with phospho-STAT3 (Tyr705), total STAT3, xCT and actin antibodies described previously[25] using total cell lysates prepared from T47D cells cultured in serum-free RPMI supplemented with vehicle (diluents only), 1.94 μM or 3.87 μM of DR-1–55 for 6 h and 24 h. Quantification of protein levels was assessed relative to actin, normalized to vehicle at each time point, for $n = 2$ cultures.

### Isolation of total RNA and quantitative RT-PCR

After end point sacrifice through exsanguination via intracardiac puncture coupled with cervical dislocation, the tumour-bearing limb was flash-frozen in liquid nitrogen and stored at −80°C. Once X-rays were taken, total RNA was extracted using a method optimized for bone based on homogenization in liquid nitrogen-chilled Trizol reagent (Life Technologies) paired with Qiagen RNeasy mini column clean-up.[28] DNase (Ambion)-treated RNA was spectrophotometrically quantified and cDNA was synthesized from a standardized final concentration of 3 μg of total RNA per reaction using Superscript III Reverse Transcriptase (Life Technologies) according to

the manufacturer's protocol. Quantitative polymerase chain reaction (qPCR) was carried out using SsoAdvanced Universal SYBR Green Supermix (Bio-Rad) and the CFX Connect Detection System (Bio-Rad). Each qPCR reaction (12.5 μL) consisted of a 1×Master Mix with 0.04 μM of forward and reverse primers and 1:3 diluted cDNA, with all samples assayed in duplicate. Amplification of specific products was performed by initial denaturation at 95°C, followed by 40 cycles of 95°C for 5 s and 60°C for 15 s. Data were normalized to the appropriate housekeeping gene (Table 1) using the 2-[Δ][Δ]Ct method.[29,30]

### Enzyme-linked immunosorbent assay

A human IL-6 enzyme-linked immunosorbent assay (ELISA) with no species cross-reactivity (R&D Systems, D6050) was used to measure levels of this tumour-derived cytokine in murine serum samples collected from all animals at experimental end point. Whole blood collected from each anaesthetized mouse via intracardiac bleed into a covered test tube (approximately 500 μL per animal) was allowed to clot undisturbed at room temperature for 30 min, followed by centrifugation at 2000*g* for 10 min at 4°C. The serum supernatant was immediately transferred into a clean Eppendorf tube and stored at −80°C. Duplicate 90 μL aliquots of each sample, thawed on ice, were each mixed with 10 μL of assay diluent, and the resulting 100 μL were loaded into wells of the 96-well ELISA plate. The assay was carried out according to the manufacturer's protocol alongside a set of serially diluted standards, assessed in duplicate.

### Statistical analyses

Statistical differences between in vitro treatment groups were determined by *t* test (denoted by stars) or a 1-way analysis of variance (ANOVA) with a Tukey's post hoc test (denoted by different letters) using GraphPad Prism software. For in vivo behavioural data, a 2-way ANOVA with a Bonferroni post hoc test was selected to compare between treatment groups over time (stars are indicated for significant differences at a specific time point). For all analyses, results were considered significant at $p < 0.05$ and are represented with standard error of the means (SEM).

## Results

MDA-MB-231 and T47D clones previously characterized for changes in pSTAT3 and xCT protein levels relative to passage-matched wild-type counterparts[25] were cultured in the absence of continuous SH-4–54 administration. Consistent with previous findings in which clones were cultured with SH-4–54, extracellular glutamate levels were 2-fold lower in MDA-MB-231 clones ($p = 0.007$), while in T47D clones, levels increased by five-fold ($p = 0.0008$), relative to respective wild-type parental cells (Figure 1(a)). A secretome analysis of these cell lines was also carried out, given that IL-6 was recently identified as a cytokine associated with CIBP in a rat breast cancer model.[31] While not statistically significant, secreted IL-6 levels were 5.3-fold lower in MDA-MB-231 clones relative to wild-type cells (from $2.2 \times 10^{-4}$ for the wild-type to $4 \times 10^{-5}$ for the clone, $p = 0.1124$; Figure 1(b)). In contrast, IL-6 levels increased significantly by 200-fold, from $3.3 \times 10^{-7}$ pg/mL/cell in conditioned media collected from T47D wild-type cells to over $6.7 \times 10^{-5}$ pg/mL/cell in the high pSTAT3/xCT-expressing T47D clone group ($p = 0.0097$; Figure 1(b)). In addition, IL-1β secretion was also significantly up-regulated by 2.8-fold in T47D clones relative to their wild-type cells ($p < 0.05$; Figure 1(c)). Extracellular glutamate profiles, coupled with the release of several known pro-nociceptive cytokines, supported our strategy to target STAT3/xCT in cells comprising a bone tumour as a means to ameliorate CIBP.

Subcutaneously injected MDA-MB-231 clones give rise to tumour xenografts that are 20-fold smaller in volume relative to those initiated from wild-type counterparts (a grain of rice compared to a marble, respectively).[25] This difference in growth potential is in line with reports that system $x_c^-$ is essential for the growth and survival of particularly aggressive cancers. However, in order to circumvent the possible experimental pitfall that slower growing MDA-MB-231 clones might not

**Table 1.** Human qPCR primers used to detect mRNA levels of each target.

| Human target gene | Forward (5′–3′) | Reverse (5′–3′) | Melt peak (°C) |
|---|---|---|---|
| *xCT* (*SLC7A11*)* | CCT CTA TTC GGA CCC ATT TAG T | CTG GGT TTC TTG TCC CAT ATA A | 79.5–80.0 |
| *IL6*** | ACT CAC CTC TTC AGA ACG AAT TG | CCA TCT TTG GAA GGT TCA GGT TG | 82.5–83.0 |
| *IL1B** | ATG ATG GCT TAT TAC AGT GGC AA | GTC GGA GAT TCG TAG CTG GA | 84.0–84.5 |
| *MYC** | GTC AAG AGG CGA ACA CAC AAC | TTG GAC GGA CAG GAT GTA TGC | 84.5–85.0 |
| Actin* | GGT CAT CAC CAT TGG CAA TG | GGT AGT TTC GTG GAT GCC ACA | 89.0–89.5 |
| RPII-2** | GAA ACG GTG GAC GTG CTT AT | TCT CCA TGC CAT ACT TGC AC | 87.5–88.0 |

Note: Human housekeeping gene primers are underlined; asterisks denote which targets were paired with efficiency-tested housekeepers for ΔCt calculations.

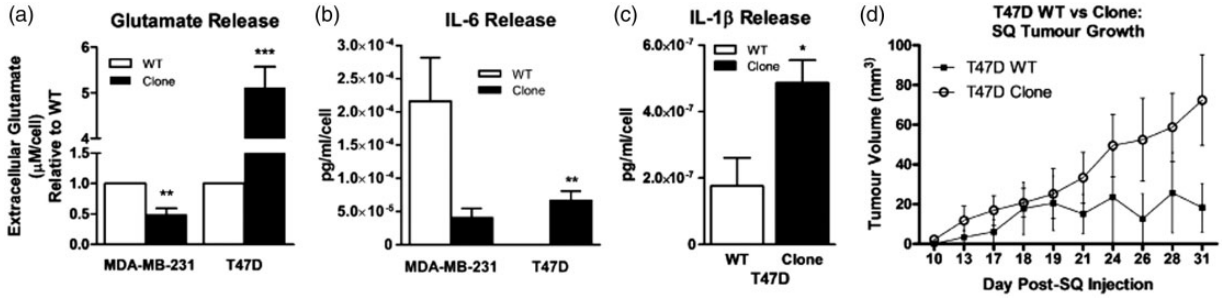


**Figure 1.** The xCT/pSTAT3 profile influences extracellular glutamate and cytokine levels in two different human breast cancer cell lines clonally derived through chronic SH-4–54 treatment. (a) Glutamate, (b) IL-6 and (c) IL-1$\beta$ release. Data were obtained from media collected from n = 3 independently cultured wild-type (WT) and SH-4–54-resistant (Clone) MDA-MB-231 and T47D cells, with ** corresponding to $p < 0.01$ and *** to $p < 0.001$. (d) Subcutaneous injection of T47D Clones into nude mice revealed differences in their growth rate compared to WT counterparts. Although not statistically significant, a four-fold larger mean tumour volume was recorded using n = 4 animals per group.

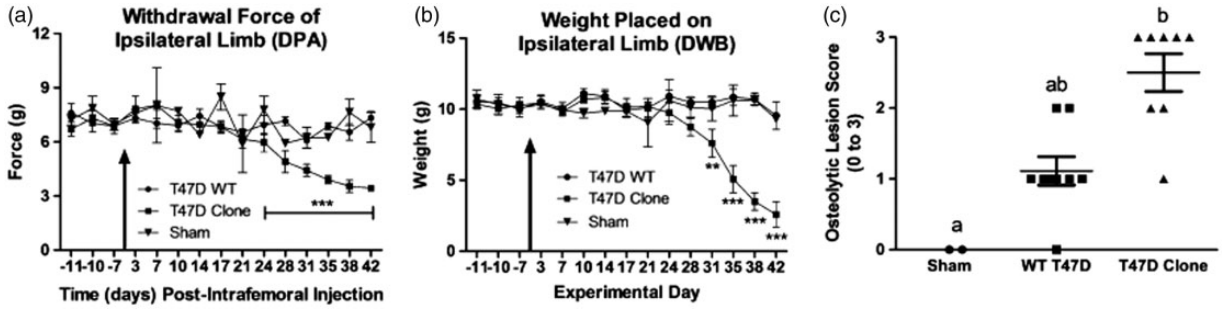


**Figure 2.** The intrafemoral presence of a bone tumour derived from a T47D human breast cancer cell line over-expressing xCT/pSTAT3 evokes significant nociceptive behaviours in a CIBP xenograft model. (a) Withdrawal force measured in grams (g) of the tumour-bearing hind paw in response to a progressive stimulus (the DPA filament) applied to the plantar surface. Statistically significant differences were observed beginning at day 24 between animals with a bone tumour initiated from T47D wild-type (WT) and the SH-4–54-resistant, xCT/pSTAT3-overexpressing cell line (Clone). WT tumours did not differ from heat/freeze-thaw treated clones (no tumour, Sham). (b) Weight (g) distributed on the tumour-bearing limb, assessed in the DWB test, was significantly different beginning at day 31 between WT and clonal groups, with animals intrafemorally injected with WT cells maintaining postural equilibrium for a longer period of time during the later stages of bone tumour development. In (a) and (b), the arrow indicates the day at which cancer cells were intrafemorally injected, corresponding to day 0, and data represent the mean $\pm$ the standard error of the mean for each group, with ** corresponding to $p < 0.01$ and *** to $p < 0.001$. (c) A graphical representation of radiographic lesion scores (0–3) for individual animals in each bone tumour group. Although not statistically significant, bone tumours induced by intrafemoral injection of clones were associated with a higher incidence of osteolysis than those induced by the presence of WT cells, with letters denoting statistical differences between groups. Sham animals showed no loss of bone density. Results in (a), (b) and (c) represent n = 8 animals for T47D WT and Clone, and n = 2 for Sham.

become established in the bone microenvironment, T47D clones were assessed as subcutaneous tumour xenografts, with wild-type cells and clones growing at similar rates until approximately day 21 post-injection (Figure 1(d)). Although not statistically significant, a four-fold difference in tumour volume (18.3 $mm^3$ for wild-types vs. 72.4 $mm^3$ for clones) was observed between groups at end point (Figure 1(d)), and this set of cells was selected to establish a CIBP xenograft model to assess nociceptive behaviours.

Mice intrafemorally injected with T47D clones demonstrated significantly more nociceptive behaviours relative to animals injected with wild-type cells using the DPA (Figure 2(a)) and DWB (Figure 2(b)) tests ($P < 0.0001$, two-way ANOVA with a Bonferroni post hoc), with the sham not differing statistically from the wild-type group. Nociception first emerged at day 24 with the DPA test, with the force required to withdraw the tumour-bearing paw being $6.94 \pm 0.53$ g in the wild-type vs. $5.97 \pm 0.53$ g in the clone-initiated tumour group ($p < 0.001$), although the difference in weight placed on the tumour-bearing limb ($10.91 \pm 0.45$ g in the wild-type vs. $9.74 \pm 0.79$ g in the clone) was not significant at this time point, likely due to differences in the threshold sensitivity detected by each test. Radiography revealed that, although not statistically significant (1-way ANOVA coupled with a Tukey's post hoc), T47D wild-type-derived tumours induced bone lesions that were less

severe than those initiated from T47D clones (Figure 2 (c); mean osteolytic lesion scores of 1.25 vs. 2.5, respectively), with results confirmed by H&E staining (data not shown).

After establishing that bone tumours initiated from T47D clones did induce significant nociceptive responses, the efficacy of DR-1–55, a novel STAT3 inhibitor, the structure of which is shown in Figure 3 (a), was assessed. This particular molecule was selected based on pharmacokinetic analyses (Figure 3(b), Table 2) demonstrating enhanced in vivo stability and bioavailability compared to SH-4–54.[27] Whereas DR-1–55, which selectively targets STAT3 relative to STAT5, did not significantly alter the number of wild-type T47D cells at any of the selected concentrations (Figure 3(c)), T47D clone numbers were significantly reduced at 3.87 μM (Figure 3(d)). Blocking pSTAT3 increases the levels of ROS, evoking an acute survival mechanism to regain redox homeostasis through *xCT* up-regulation/increased system $x_c^-$ activity similar to what we have previously observed with SH-4–54[32] as well as with capsazepine, an agent that blocks cystine uptake in vitro.[13] Therefore, a time point not associated with high ROS or reduced cell numbers was selected to assess changes in xCT expression. Under serum-free conditions after a 6 h culture, xCT protein levels were reduced by approximately 30% relative to vehicle-treated cells, correlating with a 20% reduction in total STAT3 levels in response to a 3.87 μM concentration of DR-1–55 (Figure 3(e)). A decline in total STAT3 levels correlating with reduced pSTAT3 levels in response to DR-1–55 is in line with the effects reported for this particular class of compounds, which also includes BP-1–102 and AC-3–19, two molecules that have been shown to specifically bind to and induce the degradation of STAT3 in thermal shift assays.[33] After 24 h, 1.94 μM of DR-1–55 affected total STAT3 levels similarly to the 3.87 μM concentration at 6 h, with xCT protein levels beginning to rise as cells first began to "round up," a sign of cellular stress.[34] Lysates from cells treated with 3.87 μM of DR-1–55 at

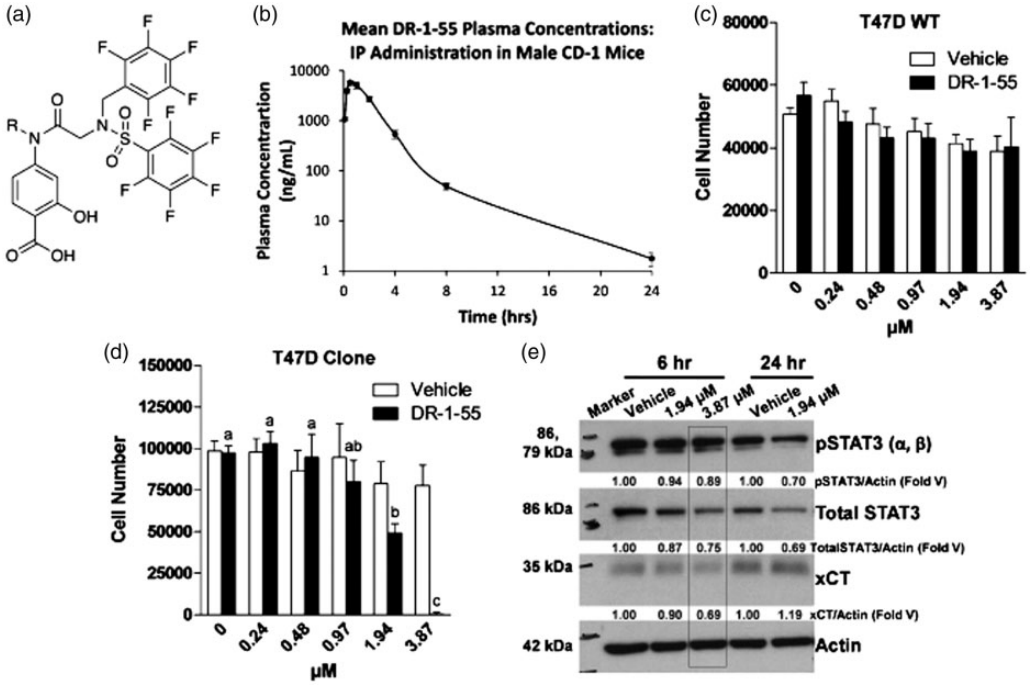


**Figure 3.** The novel STAT3 inhibitor DR-1–55 affects cell growth and down-regulates xCT and total STAT3 protein levels in a T47D human breast cancer cell line over-expressing xCT/pSTAT3. (a) A diagrammatic representation of the structure of DR-1–55 and (b) its in vivo pharmacokinetics assessed in CD-1 male mice (n = 3) following IP injection with a 25 mg/mL concentration at selected time points ranging from 5 min to 24 h. (c) A range of concentrations of DR-1–55 failed to affect T47D wild-type (WT) cell numbers after a 72-h culture in the presence of this small molecule inhibitor, while (d) the T47D SH-4–54-resistant, xCT/pSTAT3-overexpressing cell line (Clone) were sensitive, with a significant reduction in cell number beginning at approximately 2 μM. Letters denote statistical differences between groups. In (a) and (b), results represent n = 3 independent experiments. (e) As few cells remained at 72 h post-treatment and xCT levels are highly influenced by cell stress, DR-1–55 target validation at 1.94 and 3.87 μM was confirmed by Western blotting at 6 h and 24 h, revealing an approximate 30% reduction of xCT protein levels at 3.87 μM, which corresponded with a 20% reduction of total STAT3 relative to vehicle. Note that pSTAT3 (86 and 79 kDa), xCT (35 kDa) and actin (42 kDa) were co-detected on the same membrane, while total STAT3 (86 kDa) was detected post-strip. Numerical values represent densitometric analyses expressed relative to actin as a fold of vehicle-treated cells at each time point, with data obtained from n = 2 independent experiments.

**Table 2.** Pharmacokinetics of DR-1–55 (25 mg/kg) administered by intraperitoneal injection in CD-1 male mice (n = 3).

| Animal | $t_{1/2}$ (h) | $t_{max}$ (h) | $C_{max}$ (ng/mL) | $AUC_{last}$ (h·ng/mL) | $AUC_{Inf}$ (h·ng/mL) | AUC Extr (%) | MRT (h) | AUC/D (h·mg/mL) |
|---|---|---|---|---|---|---|---|---|
| 1 | 2.45 | 0.500 | 6090 | 13,769 | 13,773 | 0.0321 | 1.77 | 688 |
| 2 | 2.69 | 0.500 | 5070 | 11,892 | 11,899 | 0.0561 | 1.82 | 595 |
| 3 | 2.70 | 0.500 | 6120 | 14,028 | 14,037 | 0.0630 | 1.89 | 701 |
| Mean | 2.61 | 0.500 | 5760 | 13,230 | 13,236 | 0.0504 | 1.83 | 661 |
| SD | 0.14 | 0.000 | 598 | 1165 | 1166 | 0.0162 | 0.06 | 58 |
| CV% | 5.38 | 0.000 | 10.4 | 8.81 | 8.81 | 32.2 | 3.09 | 8.81 |

AUC: area under the curve; SD: standard deviation; CV: coefficient of variation; MRT: mean residence time.

24 h were not prepared, as a proportion of cells at this higher concentration had detached from the plate by this time.

We next evaluated whether DR-1–55 administration elicited anti-nociceptive effects in the T47D clone CIBP xenograft model. Daily IP injections were initiated at day 21 post-intrafemoral cancer cell implantation, as the emergence of nociceptive behaviours for this particular cell line first begins to be apparent at day 24 (Figure 2(a)). A 25 mg/kg daily dose of DR-1–55 was selected based on its in vivo pharmacokinetics (Figure 3(b), Table 2) and analysis of a wild-type MDA-MB-231 subcutaneous tumour xenograft study demonstrating that this concentration halts tumour growth seven days after the first IP injection of this agent (data not shown). DR-1–55-treated tumour-bearing animals presented with a significantly delayed onset and reduced severity of nociceptive behaviours relative to vehicle-treated counterparts across all three tests, an effect that was not observed between sham animals (Figure 4, compare right vs. left panels, respectively). For the DPA analysis (Figure 4(a)), the force required to induce paw withdrawal of the tumour-bearing limb was significantly higher on day 29 in the DR-1–55-treated relative to the vehicle-treated tumour-bearing group (two-way ANOVA with a Bonferroni post hoc; $4.86 \pm 0.68$ g vs. $7.14 \pm 0.47$ g, respectively, $p < 0.05$,). The paw withdrawal force recorded between groups was not statistically significant at day 32 ($4.43 \pm 0.65$ g vs. $6.52 \pm 1.14$ g, respectively). The DPA test also indicated that DR-1–55-treated tumour-bearing animals did not differ in their responses from combined shams (n = 3) at any of the experimental time points. Similarly, a two-way ANOVA with a Bonferroni post hoc of the DWB data (Figure 4(b)) revealed significant, approximately two-fold increases ($p < 0.01$) in weight borne on the tumour-bearing limb of DR-1–55-treated animals relative to those treated with vehicle on experimental day 29 ($5.05 \pm 1.44$ g vs. $8.94 \pm 0.35$ g, respectively) and day 32 ($3.93 \pm 1.31$ g vs. $8.01 \pm 1.08$ g, respectively). The DWB test also indicated that weight borne by the tumour-bearing limb of DR-1–55-treated animals did not differ from combined shams at any time point. Finally, open-field observational scoring of nociceptive behaviours demonstrated that limb favouring in mice implanted with sham cells did not statistically differ from animals with tumours initiated from T47D clones treated with DR-1–55, while tumour-bearing mice treated with vehicle were scored significantly lower relative to the DR-1–55 treatment tumour-bearing group on experimental day 29 ($2.3 \pm 0.5$ vs. $3.3 \pm 0.3$, respectively) and day 32 ($1.7 \pm 0.4$ vs. $3.3 \pm 0.7$, respectively), as assessed by two-way ANOVA with a Bonferroni post hoc ($p < 0.0001$; Figure 4(c)). T47D clone-derived tumour-bearing animals that did not exhibit osteolytic lesions at either day 28 (Figure 5(a)) or end point (Figure 5(b)) due either to a tumour outside of the femur or a flawed bone injection on day 0 were excluded from final analyses and were not included in any of the behavioural results summarized in Figure 4. Final animal numbers, from an initial n = 8, were n = 7 for the vehicle-treated tumour-bearing group, n = 6 for the DR-1–55-treated tumour-bearing group and n = 3 for combined shams (n = 1 for an untreated sham animal, n = 1 for a sham injected with vehicle, and n = 1 for a sham injected with DR-1–55. No statistically significant differences were observed between lesion scores of animals treated with vehicle or DR-1–55 at either experimental time point (Figure 5(a) and (b)).

The average daily body weight of all animals was recorded, starting at the baseline (day 4) until end point (Figure 5(c)). The presence of a bone tumour evoked an expected drop in body weight, irrespective of treatment (compare total grams at day 15 and end point; vehicle: $26.9 \pm 0.5$ g vs. $25.1 \pm 0.5$ g, $p = 0.028$; DR-1–55: $26.9 \pm 0.9$ g vs. $23.8 \pm 0.6$ g, $p = 0.0034$). Although not statistically significant, a 7% reduction in total body weight was observed four days after first initiating daily IP injections between the two treatment groups ($25.9 \pm 0.5$ g for vehicle vs. $24.1 \pm 0.7$ g for DR-1–55, $p = 0.06$). The cause of this difference in weight loss remains to be determined, although, based on animal skin condition, it could be attributed to DR-1–55-induced dehydration. After conferring with CAF

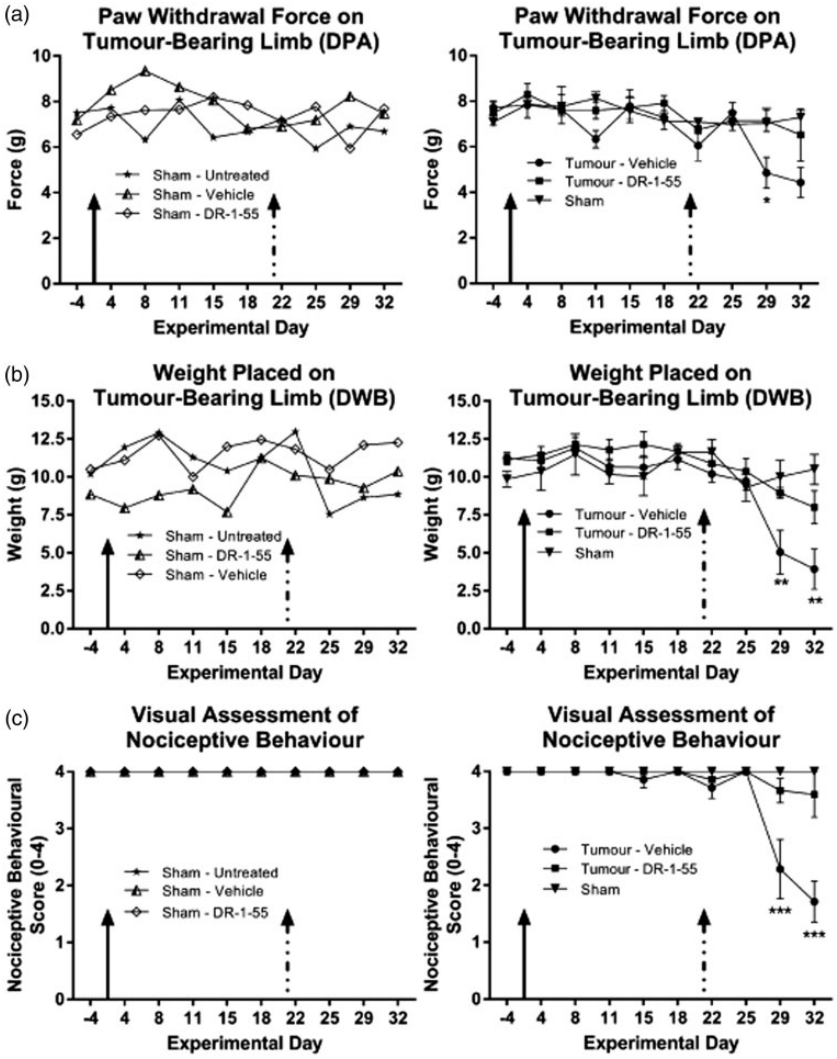


**Figure 4.** DR-1–55 significantly delays the onset of nociceptive behavioural responses relative to vehicle-treated animals with CIBP. Mice were inoculated with T47D SH-4–54-resistant, xCT/pSTAT3-overexpressing cells or heat-inactivated cancer cells (shams) on day 0 (solid arrow). Treatments administered via daily IP injections were initiated on day 21 (dashed arrow). Left panels for (a) to (c) represent ungrouped behavioural results for each sham animal, while right panels represent data for a grouped sham compared to tumour-bearing mice without (vehicle-treated) and with DR-1–55. (a) Hind paw withdrawal force in grams (g) was significantly different on day 29 between the DR-1–55- and vehicle-treated tumour-bearing groups, with the latter being more sensitive to a lower filament pressure, indicating a delay in the onset of evoked nociceptive behaviour. (b) Gram weight (g) distributed on the tumour-bearing limb, assessed in the DWB test, was significantly different on day 29 and 32 between the DR-1–55- and vehicle-treated groups, with animals injected with DR-1–55 maintaining postural equilibrium for a longer period of time. (c) Open-field observational scoring of nociceptive behaviours based on a predefined 0–4 visual pain scale in which a 4 represents no indication of distress. Significant differences were observed on day 29 and 32 between tumour-bearing DR-1–55- and vehicle-treated mice. Results in (a) to (c) represent $n = 7$ animals for tumour with vehicle, $n = 6$ for tumour with DR-1–55, $n = 3$ for combined Sham, $n = 1$ for Sham with vehicle, and $n = 1$ for Sham with DR-1–55. Data represent the mean $\pm$ the standard error of the mean for each group, with * corresponding to $p < 0.05$, ** to $p < 0.01$ and *** to $p < 0.001$.

staff, fluid-enriched nutrient gel packs were introduced into each cage coupled with subcutaneous fluid administration to all animals, irrespective of treatment. This intervention resulted in a recovery of mean body weight among the DR-1–55-treated group to levels that did not significantly differ from those in the vehicle-treated group (compare weights at end point). However, this unexpected in vivo effect resulted in early termination of the trial, with final behavioural measures collected at day 32.

To assess whether DR-1–55 down-regulates expression of the primary target, human *xCT*, in bone tumours, we capitalized on the CIBP xenograft model, which allowed for differentiation between human tumour mRNA and mouse host mRNA. Using RNA extracted from crushed bone and surrounding soft

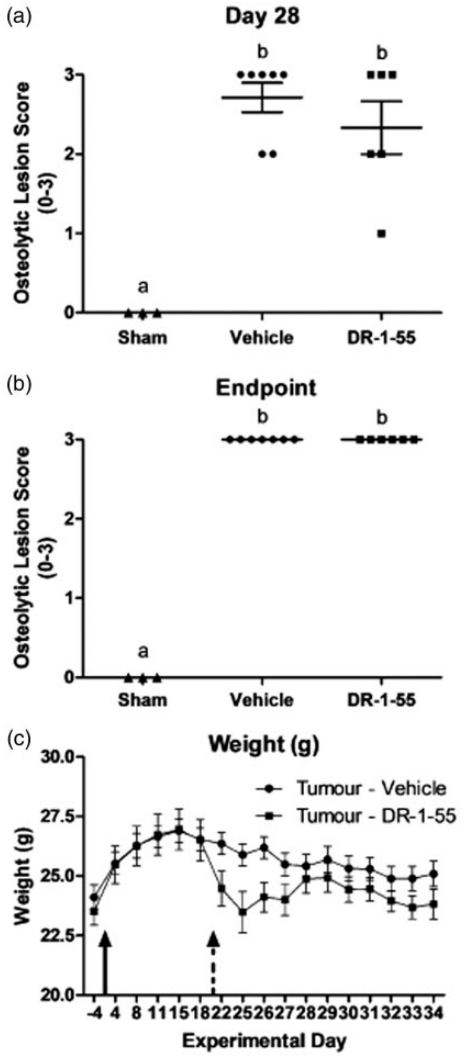


**Figure 5.** DR-1–55 does not affect osteolytic lesion size relative to lesions formed in vehicle-treated animals with CIBP. (a) day 28 and (b) day 34 graphical representations of radiographic lesion scores (0–3) for individual animals in each treatment group represented in Figure 4. No statistically significant differences were observed between animals intrafemorally injected with T47D SH-4–54-resistant, xCT/pSTAT3-overexpressing cells treated with either vehicle or DR-1–55 at either experimental time point, with both groups scoring close to 3 (high degree of osteolysis). Shams showed no loss of bone density. Letters denote statistical differences between groups. (c) Animal weight in grams (g), measured daily from the baseline until end point. No statistically significant differences were observed between groups.

tissue in tumour-bearing limbs as a cDNA source for qPCR, human *xCT* (*SLC7A11*) mRNA levels were found to be significantly down-regulated by >6-fold in animals administered with DR-1–55 for 14-days relative to the vehicle-treated group (Figure 6(a)). The upper panel in Figure 6(a) depicts the mean ΔCt values (*SLC7A11* target gene Ct values – housekeeping gene Ct values for each individual animal per treatment group), which were significantly different ($p < 0.01$). A graphical representation of the calculated relative fold changes in *xCT* mRNA levels relative to vehicle (1- vs. 0.15-fold for vehicle vs. DR-1–55-treated, respectively) is summarized in the lower panel of Figure 6(a) based on the 2-[Δ][Δ]Ct method.[29,30] Putative changes in human cytokine mRNA levels in the bone tumour that were identified to be differentially secreted by breast cancer cells (Figure 1) were also assessed. Human *IL6* mRNA levels were significantly down-regulated in response to DR-1–55 treatment by two-fold in tumour-bearing limbs relative to corresponding tissue isolated from vehicle-treated animals (1- vs. 0.47-fold, respectively, $p = 0.05$, Figure 6(b)) using the same approach employed for *xCT* described above. Data for human *IL1B* mRNA are summarized in Figure 6(c), with an approximate six-fold down-regulation in response to DR-1–55 relative to vehicle (1- vs. 0.17-fold, respectively, $p < 0.01$). In addition, as MYC is a known target of pSTAT3 previously identified to be differentially regulated in both the T47D and MDA-MB-231 wild-type/clone comparisons by NextGen sequencing,[25] changes in its expression at the mRNA level were also examined. Indeed, human *MYC* mRNA levels followed the pattern of down-regulation observed for the other genes, with its expression decreasing by five-fold in bone tissue derived from DR-1–55-treated animals relative to those treated with vehicle (1- vs. 0.2-fold, respectively, $p < 0.01$, Figure 6(d)). The standard SEM for ΔCt values was based on $n = 7$ (vehicle-treated) and $n = 6$ (DR-1–55-treated) animals.

An examination of human IL-6 levels released by the bone xenografts revealed that, similar to results reported in vitro, tumours initiated from human T47D wild-type cells released no detectable amount of this cytokine ($n = 8$; 0 pg/mL) compared to circulating human IL-6 levels detected in animals intrafemorally injected with T47D Clone cells ($n = 6$; $17.33 \pm 5.88$ pg/mL, $p = 0.0048$; Figure 7(a)), assessed at the 42 day experimental end point. In support of *IL6* mRNA data shown in Figure 6(b), DR-1–55 treatment of mice bearing a T47D Clone-initiated tumour reduced the release of IL-6 by 1.8-fold relative to results obtained for the vehicle-treated group, from $2.63 \pm 0.59$ pg/mL for the vehicle ($n = 7$) to $1.46 \pm 0.57$ pg/mL for the DR-1–55 group ($n = 7$) to a concentration that did not statistically differ from Shams lacking a viable bone xenograft (0 pg/mL, one-way ANOVA with a Tukey's post hoc test; Figure 7(b)). No human IL-6 could be detected in the serum of non-tumour-bearing sham-injected animals (Figure 7(a) and (b))

## Discussion

The development and therapeutic evaluation of STAT3 inhibitors continues to be of ongoing interest to target

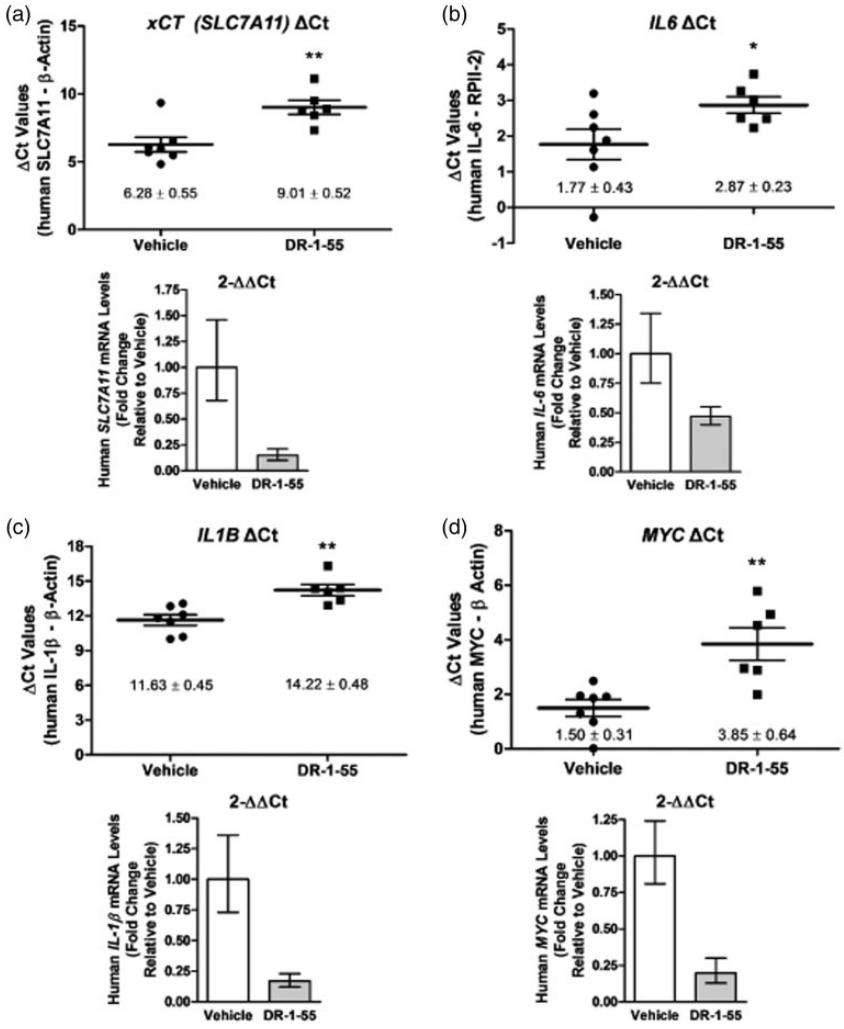


**Figure 6.** DR-1–55 treatment results in down-regulation of *xCT* and other relevant targets at the mRNA level in bone xenografts relative to tissue derived from vehicle-treated animals. Human (a) *xCT*, (b) *IL6*, (c) *IL1B* and (d) *MYC* mRNA levels, assessed by qPCR, were significantly down-regulated in the tumour-bearing limb of DR-1–55- relative to vehicle-treated animals originally implanted with T47D SH-4–54-resistant, xCT/pSTAT3-overexpressing cells. The top panels depict ΔCt (target-housekeeper) for each individual animal, represented by a dot for vehicle ($n = 7$) and a square for DR-1–55 ($n = 6$) ± the SEM, with * corresponding to $p < 0.05$ and ** to $p < 0.01$. The bottom panels provide a fold change representation relative to vehicle of the top panels based on the 2-[Δ][Δ]Ct method, demonstrating overall changes in target mRNA levels.

"difficult-to-treat" cancers, including triple-negative breast carcinomas, pancreatic cancer and gliomas, which, in addition to high pSTAT3 levels, also exhibit up-regulated xCT expression.[16,35,36] Napabucasin (BBI608), an orally available STAT3/cancer cell stemness inhibitor[37,38] currently in phase 1, 2 and 3 trials for pancreatic, colorectal and non-squamous non-small cell lung cancers (ClinicalTrials.gov), highlights the potential translational impact of the findings presented here, assessing whether a block in STAT3 pathway activation, which is positively associated with xCT expression in aggressive breast cancer cells, alters nociception in a preclinical CIBP model. Mechanisms that support *xCT* up-regulation and promote system $x_c^-$-mediated glutamate release by cells comprising a skeletal metastasis may also be inextricably linked to tumour growth. In CIBP patients, the absence of pain is generally indicative of a positive prognosis. Although it remains to be experimentally determined, changes in tumour size may reflect changes in the threshold level of a repertoire of pro-nociceptive factors released by cancer cells into the bone environment, potentially dictating the severity of pain experienced by a patient due to aberrant bone remodelling and activation of nociceptive pathways that contribute to central sensitization. Therefore, limiting tumour size could potentially also limit the release and action of pro-nociceptive factors from cancer cells, improving patient morbidity. This study evaluated the

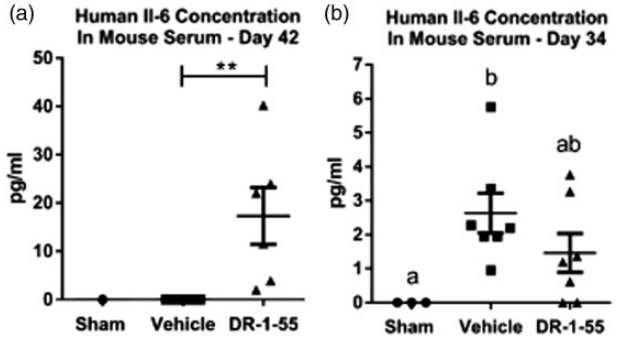


**Figure 7.** Circulating human IL-6 levels are elevated in the serum of mice bearing a tumour derived from T47D human breast cancer cell line over-expressing xCT/pSTAT3 relative to T47D wild-type cells, and DR-1–55 treatment down-regulates systemic human IL-6 levels relative to vehicle. (a) While no human IL-6 was detected in the serum of an animal injected with heat/freeze-thaw-inactivated cells (Sham) of the T47D human breast cancer cell line over-expressing xCT/pSTAT3 at the day 42 experimental end point, significantly higher levels ($p < 0.0048$) were measured in serum collected from animals intrafemorally injected with the T47D xCT/pSTAT3 over-expressing Clone ($n = 6$) relative to wild-type T47D tumour-bearing animals (WT; $n = 8$). (b) Analysis of serum collected 34 days post-intrafemoral injection of T47D clone-derived cells revealed a trend towards higher levels of human IL-6 in vehicle-treated animals ($n = 7$) relative to those treated with DR-1–55 ($n = 7$), which did not differ from Shams ($n = 3$). Data represent the mean ± the standard error of the mean for each group in pg/mL, with ** corresponding to $p < 0.005$ and letters denoting statistical differences between groups.

analgesic potential of DR-1–55, a novel agent within the class of therapeutically relevant small molecules designed to specifically target STAT3, in the context of down-regulating *xCT* mRNA levels in the bone tumour. This approach may be particularly relevant for painful tumours that have become resistant to first-line chemotherapy and/or radiation, as surviving cells often demonstrate up-regulated system $x_c^-$ activity accompanied by a significant growth advantage (reviewed in Lewerenz et al.[20]), potentially also causing severe pain. While the precise pluripotency-associated targets of napabucasin, which blocks cancer stem cell self-replication and differentiation into heterogeneous cell populations associated with malignant growth, recurrence and resistance to chemotherapy, remain to be fully defined, it would not be surprising to discover that this agent also targets *xCT* through its action on the STAT3 pathway.

Given their five-fold increase in glutamate release, we employed a T47D breast cancer cell line stably over-expressing pSTAT3 and xCT relative to parental wild-type cells as a tool to examine the effects of down-regulating *xCT*/system $x_c^-$ activity in an animal model of CIBP. Specifically, we assessed whether DR-1–55, a novel STAT3 inhibitor demonstrating extended in vivo half-life and improved bioavailability, affects nociceptive behaviours by targeting cancer cell-expressed *xCT* in vivo. In addition to delaying the onset of nociception, *xCT* mRNA levels were significantly down-regulated in bone tumours derived from DR-1–55-treated animals relative to those isolated from animals treated with vehicle. While osteolytic lesion scores, which may provide indirect cues regarding overall tumour burden, did not differ significantly between groups, it is likely that, given the four-fold subcutaneous growth advantage of xCT over-expressing T47D clones relative to parental wild-type cells, and given that DR-1–55 treatment reduced the cell number of T47D clones in vitro, this agent also impaired bone tumour growth in the CIBP model. Indeed, a recent study based on a xenograft osteosarcoma mouse model induced through intratibial human 143B cell injection reported a significant decrease in tumour volume, accompanied by weight loss and reduced incidence of lung metastases in response to IP napabucasin injection (every three days for a total of eight treatments, which were initiated two weeks post-model induction).[39] It should be noted that no radiographic images were presented by Zuo et al.,[39] and the size of each osteosarcoma was calculated based on methods designed for measuring subcutaneous tumour volume, which includes local tissue inflammation and tumour growth outside of the bone in addition to growth of cancer cells within the tibial medullary cavity.[39] Importantly, differences in tumour size will remain a significant confound in CIBP studies that target STAT3 or *xCT* down-regulation, in light of the essential role of system $x_c^-$ in supporting the growth and survival of aggressive cancer subtypes. This premise is supported by the growth-inhibitory properties of sulfasalazine, an established system $x_c^-$ inhibitor,[14] in human pancreatic cancer xenografts[17] and in a syngeneic rat lymphoma model.[18] In addition, STAT3 targets other metabolic pathways in cancer cells that are linked with cell proliferation and growth, including MYC, a well-characterized oncogene that drives cell proliferation and growth (reviewed in Miller et al.[40]).

An additional finding of the current investigation was the significant down-regulation of human *IL6* and human *IL1B* mRNA levels in bone tumours in response to DR-1–55 treatment. These encode IL-6 and IL-1β, pro-inflammatory cytokines that are differentially secreted by T47D clones relative to wild-type cells. Both of these cytokines require STAT3 tyrosine phosphorylation for their production in lipopolysaccharide-challenged murine macrophages[41] and play important roles in inflammatory diseases, cancer and pain (reviewed in Vendrell et al.[42]). Importantly, we show that not only are *IL6* mRNA levels down-regulated in the tumour xenograft, but human IL-6 protein levels derived exclusively from the bone tumour are lower in the serum of

DR-1–55-treated relative to vehicle-treated mice bearing an *xCT*-positive tumour. A recent study assessed the effects of a novel small molecule antagonist (TB-2–081) of IL-6 signalling on nociceptive behaviours, bone integrity and tumour progression in a syngeneic rat model of breast CIBP, demonstrating a significant treatment-induced reduction in osteolytic and osteoblastic bone remodelling and time-to-fracture.[31] The authors concluded that an early block of IL-6-mediated signalling using agents such as TB-2–081 represents a disease-modifying strategy that could diminish chronic CIBP.[31] In the current investigation, it is possible that bone remodelling initiated during the first several weeks following introduction of cancer cells into the head of the femur may have already reached a threshold level to induce the formation of osteolytic lesions, a process that could not be repaired upon initiation of DR-1–55 treatment 3 weeks post-cancer cell injection. Given the inter-relationship between IL-6 and STAT3 in bone metabolism,[43] earlier administration of DR-1–55 could potentially have similar effects on bone remodelling as reported for the IL-6 antagonist used by Remeniuk et al.[31] However, STAT3, as well as system $x_c^-$, are closely tied to tumour size and disease progression, and it may therefore be difficult to assess early bone remodelling as well as later CIBP-induced nociception in vivo, given that treatment with DR-1–55 at an earlier time point may inhibit tumour establishment by limiting breast cancer cell proliferation in the bone microenvironment.

Another possibility to consider in comparing the findings of the current investigation with those in the study by Remeniuk et al.[31] is that blocking STAT3 may produce different effects than targeting IL-6, which may occur in a cell type-dependent manner. In support of this notion, Yokota et al.[44] showed that conditional knockout of murine *Stat3* in osteoclast-like cells did not significantly reduce their differentiation efficiency in response to IL-6, which was unexpected, given the role of STAT3 in IL-6 signalling.[44] The study further showed that IL-6-mediated activation of the Jak/Mapk/Erk/c-fos pathway was involved, with IL-6 in combination with TNFα driving the differentiation of multinucleated cells closely resembling osteoclasts in their ability to absorb bone matrix in vitro, with the same proinflammatory cytokines inducing calvarial bone erosion in vivo.[44] While Remeniuk et al.[31] clearly demonstrated that rat IL-6 levels were elevated in the circulation as well as in bone exudates, which include multiple cell types found within bone marrow in addition to the injected rat MAT B III mammary adenocarcinoma cells, it was not shown whether the latter, which responded to IL-6 stimulation as assessed by increased STAT3 phosphorylation in vitro, also produce and release this cytokine themselves, which would then be blocked by TB-2–081. These interesting nuances in tumour-derived versus osteoclast-derived IL-6 and CIBP remain to be further elucidated.

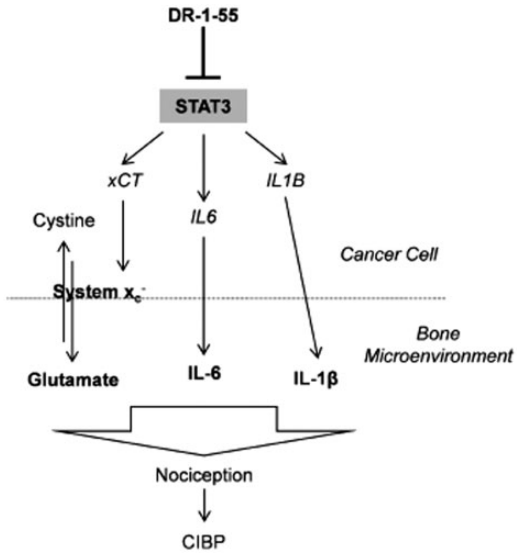


**Figure 8.** Diagrammatic summary of the putative relationship between STAT3, system $x_c^-$, IL-6 and IL-1$\beta$ in response to DR-1–55 and nociception. Agents that block STAT3 activity down-regulate the expression of specific target genes such as *xCT*, *IL6* and *IL1B* at the mRNA level in aggressive breast cancer cell subtypes with specific metabolic profiles that rely on uptake of cystine through system $x_c^-$. In turn, less glutamate is released through system $x_c^-$, and less of each cytokine (IL-6 and IL-1$\beta$) is secreted by the cell, resulting in less nociception and CIBP.

With regard to IL-1β, this cytokine activates STAT3 directly and indirectly, also inducing the expression of IL-6 family cytokines to perpetuate STAT3 activation in murine fibroblasts.[45] IL-1β has also been shown to increase the expression and extend the half-life of xCT mRNA in primary murine astrocytes.[21] In response to energy deprivation, astrocytic IL-1β contributes to glutamate-mediated neuronal injury by promoting *xCT* expression, thereby enhancing system $x_c^-$ activity (references in Shi et al.[21]). Ultimately, a combination of factors and their intracellular cross-talk, including glutamate, IL-6 and IL-1β, among others such as nerve growth factor, which itself has recently been linked to system $x_c^-$,[46] are likely modulating CIBP. Targeting a common signalling pathway mediated by, for example, STAT3 may provide a promising therapeutic approach (Figure 8).

## Conclusions and Future Directions

The current investigation is the first to employ a pSTAT3/xCT over-expression CIBP model to examine the role of STAT3 inhibition on nociceptive behaviours. The metabolic signature of breast cancer subtypes likely

dictates their production of specific pro-nociceptive factors and an exploration of the secretome profile of aggressive bone-seeking cancer cells could potentially serve as a diagnostic indicator predictive of the severity of CIBP in patients. Our results indicate that DR-1–55 elicits anti-nociceptive behavioural responses, down-regulating *xCT* as well as *IL6* and *IL1B* at the mRNA level in bone tumours initiated from a human breast cancer cell line initially expressing high levels of pSTAT3 and xCT. It will be of future interest to characterize the putative relationship between xCT, IL-6, IL-1β and STAT3, and to associate the co-release of glutamate and relevant cytokines with nociceptive responses in vivo. In addition, it will be important to assess tumour size at selected time points over the duration of a CIBP experiment and to employ a means of directly measuring the levels of secreted factors in bone exudates in response to relevant treatments at end point. Results from our investigation will hopefully provide insights for studies aimed at targeting STAT3, potentially enhancing existing clinical cancer pain management strategies, which ultimately may not differ from targeting the bone tumour itself at an as early as possible stage post-detection to avoid later central sensitization.

## Acknowledgments

The authors thank Dr. Jennifer Fazzari for her feedback on and final editing of the manuscript.

## Declaration of Conflicting Interests

The author(s) declared no potential conflicts of interest with respect to the research, authorship, and/or publication of this article.

## Funding

The author(s) disclosed receipt of the following financial support for the research, authorship, and/or publication of this article: The research of GS is funded by grants from the Canadian Institutes of Health Research (CIHR) and the Canadian Breast Cancer Foundation (CBCF). The research of PG, a Canada Research Chair, is funded by CIHR, CBCF and Canadian Foundation for Innovation grants.

## References

1. McGuire S. World Cancer Report 2014. Geneva, Switzerland: World Health Organization, International Agency for Research on Cancer, WHO Press, 2015. *Adv Nutr* 2016; 7: 418–419.
2. van den Beuken-van Everdingen MH, de Rijke JM, Kessels AG, Schouten HC, van Kleef M and Patijn J. Prevalence of pain in patients with cancer: a systematic review of the past 40 years. *Ann Oncol* 2007; 18: 1437–1449.
3. Breivik H, Cherny N, Collett B, de Conno F, Filbet M, Foubert AJ, Cohen R and Dow L. Cancer-related pain: a pan-European survey of prevalence, treatment, and patient attitudes. *Ann Oncol* 2009; 20: 1420–1433.
4. Puetzler J, Feldmann RE Jr, Brascher AK, Gerhardt A and Benrath J. Improvements in health-related quality of life by comprehensive cancer pain therapy: a pilot study with breast cancer outpatients under palliative chemotherapy. *Oncol Res Treat* 2014; 37: 456–462.
5. Mantyh PW. Bone cancer pain: from mechanism to therapy. *Curr Opin Support Palliat Care* 2014; 8: 83–90.
6. van den Beuken-van Everdingen MH, Hochstenbach LM, Joosten EA, Tjan-Heijnen VC and Janssen DJ. Update on prevalence of pain in patients with cancer: systematic review and meta-analysis. *J Pain Sympt Manag* 2016; 51: 1070–1090.e9.
7. Haumann J, Joosten EBA and Everdingen M. Pain prevalence in cancer patients: status quo or opportunities for improvement? *Curr Opin Support Palliat Care* 2017; 11: 99–104.
8. Coleman RE. Skeletal complications of malignancy. *Cancer* 1997; 80: 1588–1594.
9. Mantyh P. Bone cancer pain: causes, consequences, and therapeutic opportunities. *Pain* 2013; 154: S54–S62.
10. Seidlitz EP, Sharma MK and Singh G. Extracellular glutamate alters mature osteoclast and osteoblast functions. *Can J Physiol Pharmacol* 2010; 88: 929–936.
11. Cairns BE, Gambarota G, Svensson P, Arendt-Nielsen L and Berde CB. Glutamate-induced sensitization of rat masseter muscle fibers. *Neuroscience* 2002; 109: 389–399.
12. Fazzari J, Linher-Melville K and Singh G. Tumour-derived glutamate: linking aberrant cancer cell metabolism to peripheral sensory pain pathways. *Curr Neuropharmacol* 2017; 15: 620–636.
13. Fazzari J, Balenko MD, Zacal N and Singh G. Identification of capsazepine as a novel inhibitor of system xc- and cancer-induced bone pain. *J Pain Res* 2017; 10: 915–925.
14. Ungard RG, Seidlitz EP and Singh G. Inhibition of breast cancer-cell glutamate release with sulfasalazine limits cancer-induced bone pain. *Pain* 2014; 155: 28–36.
15. Slosky LM, BassiriRad NM, Symons AM, Thompson M, Doyle T, Forte BL, Staatz WD, Bui L, Neumann WL, Mantyh PW, Salvemini D, Largent-Milnes TM and Vanderah TW. The cystine/glutamate antiporter system xc- drives breast tumor cell glutamate release and cancer-induced bone pain. *Pain* 2016; 157: 2605–2616.
16. Timmerman LA, Holton T, Yuneva M, Louie RJ, Padró M, Daemen A, Hu M, Chan DA, Ethier SP, van 't Veer LJ, Polyak K, McCormick F and Gray JW. Glutamine sensitivity analysis identifies the xCT antiporter as a common triple-negative breast tumor therapeutic target. *Cancer Cell* 2013; 24: 450–465.
17. Lo M, Ling V, Low C, Wang YZ and Gout PW. Potential use of the anti-inflammatory drug, sulfasalazine, for targeted therapy of pancreatic cancer. *Curr Oncol* 2010; 17: 9–16.
18. Gout PW, Buckley AR, Simms CR and Bruchovsky N. Sulfasalazine, a potent suppressor of lymphoma growth by inhibition of the x(c)- cystine transporter: a new action for an old drug. *Leukemia* 2001; 15: 1633–1640.

19. Ungard RG, Seidlitz EP and Singh G. Oxidative stress and cancer pain. *Can J Physiol Pharmacol* 2013; 91: 31–37.
20. Lewerenz J, Hewett SJ, Huang Y, Lambros M, Gout PW, Kalivas PW, Massie A, Smolders I, Methner A, Pergande M, Smith SB, Ganapathy V, and Maher P. The cystine/glutamate antiporter system x(c)(-) in health and disease: from molecular mechanisms to novel therapeutic opportunities. *Antioxid Redox Signal* 2013; 18: 522–555.
21. Shi J, He Y, Hewett SJ and Hewett JA. Interleukin 1beta regulation of the system xc- substrate-specific subunit, xCT, in primary mouse astrocytes involves the RNA-binding protein HuR. *J Biol Chem* 2016; 291: 1643–1651.
22. Yu H, Pardoll D and Jove R. STATs in cancer inflammation and immunity: a leading role for STAT3. *Nat Rev Cancer* 2009; 9: 798–809.
23. Linher-Melville K and Singh G. The complex roles of STAT3 and STAT5 in maintaining redox balance: lessons from STAT-mediated xCT expression in cancer cells. *Mol Cell Endocrinol* 2017; 451: 40–52.
24. Linher-Melville K, Haftchenary S, Gunning P and Singh G. Signal transducer and activator of transcription 3 and 5 regulate system Xc- and redox balance in human breast cancer cells. *Mol Cell Biochem* 2015; 405: 205–221.
25. Linher-Melville K, Nashed MG, Ungard RG, Haftchenary S, Rosa DA, Gunning PT and Singh G. Chronic inhibition of STAT3/STAT5 in treatment-resistant human breast cancer cell subtypes: convergence on the ROS/SUMO pathway and its effects on xCT expression and system xc- activity. *PLoS One* 2016; 11: e0161202.
26. Haftchenary S, Luchman HA, Jouk AO, Veloso AJ, Page BDG, Cheng XR, Dawson SS, Grinshtein N, Shahani VM, Kerman K, Kaplan DR, Griffin C, Aman AM, Al-Awar R, Weiss S and Gunning PT. Potent targeting of the STAT3 protein in brain cancer stem cells: a promising route for treating glioblastoma. *ACS Med Chem Lett* 2013; 4: 1102–1107.
27. Ali AM, Gómez-Biagi RF, Rosa DA, Lai P-S, Heaton WL, Park JS, Eiring AM, Vellore NA, de Araujo ED, Ball DP, Shouksmith AE, Patel AB, Deininger MW, O'Hare T and Gunning PT. Disarming an electrophilic warhead: retaining potency in tyrosine kinase inhibitor (TKI)-resistant CML lines while circumventing pharmacokinetic liabilities. *ChemMedChem* 2016; 11: 850–861.
28. Carter LE, Kilroy G, Gimble JM and Floyd ZE. An improved method for isolation of RNA from bone. *BMC Biotechnol* 2012; 12: 5.
29. Livak KJ and Schmittgen TD. Analysis of relative gene expression data using real-time quantitative PCR and the 2(-Delta Delta C(T)) method. *Methods* 2001; 25: 402–408.
30. Schmittgen TD and Livak KJ. Analyzing real-time PCR data by the comparative C(T) method. *Nat Protoc* 2008; 3: 1101–1108.
31. Remeniuk B, King T, Sukhtankar D, Nippert A, Li N, Li F, Cheng K, Rice KC and Porreca F. Disease modifying actions of interleukin-6 blockade in a rat model of bone cancer pain. *Pain* 2018; 159: 684–698.
32. Linher-Melville K, Haftchenary S, Gunning P and Singh G. Signal transducer and activator of transcription 3 and 5 regulate system Xc- and redox balance in human breast cancer cells. *Mol Cell Biochem* 2015; 405: 205–221.
33. de Araujo ED, Manaswiyoungkul P, Israelian J, Park J, Yuen K, Farhangi S, Berger-Becvar A, Abu-Jazar L and Gunning PT. High-throughput thermofluor-based assays for inhibitor screening of STAT SH2 domains. *J Pharmaceut Biomed Anal* 2017; 143: 159–167.
34. Fulda S, Gorman AM, Hori O and Samali A. Cellular stress responses: cell survival and cell death. *Int J Cell Biol* 2010; 2010: 214074.
35. Chung WJ, Lyons SA, Nelson GM, Hamza H, Gladson CL, Gillespie GY and Sontheimer H. Inhibition of cystine uptake disrupts the growth of primary brain tumors. *J Neurosci* 2005; 25: 7101–7110.
36. Lo M, Ling V, Wang YZ and Gout PW. The xc- cystine/glutamate antiporter: a mediator of pancreatic cancer growth with a role in drug resistance. *Br J Cancer* 2008; 99: 464–472.
37. Li Y, Rogoff HA, Keates S, Gao Y, Murikipudi S, Mikule K, Leggett D, Li W, Pardee AB and Li CJ. Suppression of cancer relapse and metastasis by inhibiting cancer stemness. *Proc Natl Acad Sci USA* 2015; 112: 1839–1844.
38. Zhang Y, Jin Z, Zhou H, Ou X, Xu Y, Li H, Liu C and Li B. Suppression of prostate cancer progression by cancer cell stemness inhibitor napabucasin. *Cancer Med* 2016; 5: 1251–1258.
39. Zuo D, Shogren KL, Zang J, Jewison DE, Waletzki BE, Miller AL II, Okuno SH, Cai Z, Yaszemski MJ and Maran A. Inhibition of STAT3 blocks protein synthesis and tumor metastasis in osteosarcoma cells. *J Exp Clin Cancer Res* 2018; 37: 244.
40. Miller DM, Thomas SD, Islam A, Muench D and Sedoris K. c-Myc and cancer metabolism. *Clin Cancer Res* 2012; 18: 5546–5553.
41. Samavati L, Rastogi R, Du W, Huttemann M, Fite A and Franchi L. STAT3 tyrosine phosphorylation is critical for interleukin 1 beta and interleukin-6 production in response to lipopolysaccharide and live bacteria. *Mol Immunol* 2009; 46: 1867–1877.
42. Vendrell I, Macedo D, Alho I, Dionisio MR and Costa L. Treatment of cancer pain by targeting cytokines. *Mediators Inflamm* 2015; 2015: 984570
43. Li J. JAK-STAT and bone metabolism. *JAKSTAT* 2013; 2: e23930.
44. Yokota K, Sato K, Miyazaki T, Kitaura H, Kayama H, Miyoshi F, Araki Y, Akiyama Y, Takeda K and Mimura T. Combination of tumor necrosis factor alpha and interleukin-6 induces mouse osteoclast-like cells with bone resorption activity both in vitro and in vivo. *Arthritis Rheumatol* 2014; 66: 121–129.
45. Mori T, Miyamoto T, Yoshida H, Asakawa M, Kawasumi M, Kobayashi T, Morioka H, Chiba K, Toyama Y and Yoshimura A. IL-1beta and TNFalpha-initiated IL-6-STAT3 pathway is critical in mediating inflammatory cytokines and RANKL expression in inflammatory arthritis. *Int Immunol* 2011; 23: 701–712.
46. Miladinovic T, Ungard RG, Linher-Melville K, Popovic S and Singh G. Functional effects of TrkA inhibition on system xC(-)-mediated glutamate release and cancer-induced bone pain. *Mol Pain* 2018; 14: 174480691877646.